AGU PUBLICATIONS

Water Resources Research

RESEARCH ARTICLE
10.1002/2014WR016431

Special Section:
Eco-hydrology of Semiarid Environments: Confronting Mathematical Models with Ecosystem Complexity

The influence of water table depth and the free atmospheric state on convective rainfall predisposition

Sara Bonetti[1], Gabriele Manoli[1,2], Jean-Christophe Domec[3,4], Mario Putti[2], Marco Marani[1,5], and Gabriel G. Katul[1]

[1]Nicholas School of the Environment and Pratt School of Engineering, Duke University, Durham, North Carolina, USA, [2]Department of Mathematics, University of Padova, Padova, Italy, [3]Department of Forestry and Environmental Resources, North Carolina State University, Raleigh, North Carolina, USA, [4]Bordeaux Sciences Agro UMR 1391 INRA-ISPA, University of Bordeaux, Gradignan, France, [5]Department of Civil, Architectural and Environmental Engineering, University of Padova, Padova, Italy

Key Points:
- Water Table affects Convective Rainfall (CR) via the plant-atmosphere continuum
- Feedbacks from the Free Atmosphere (FA) can dominate CR for wet FA states
- Vegetation can control CR for relatively dry FA states

Supporting Information:
- Bonetti_Supporting Information
- TS01_abbreviation

Correspondence to:
S. Bonetti,
sara.bonetti@duke.edu

Citation:
Bonetti, S., G. Manoli, J.-C. Domec, M. Putti, M. Marani, and G. G. Katul (2015), The influence of water table depth and the free atmospheric state on convective rainfall predisposition, *Water Resour. Res.*, *51*, 2283–2297, doi:10.1002/2014WR016431.

Received 19 SEP 2014
Accepted 5 MAR 2015
Accepted article online 16 MAR 2015
Published online 11 APR 2015

Abstract A mechanistic model for the soil-plant system is coupled to a conventional slab representation of the atmospheric boundary layer (ABL) to explore the role of groundwater table (WT) variations and free atmospheric (FA) states on convective rainfall predisposition (CRP) at a Loblolly pine plantation site situated in the lower coastal plain of North Carolina. Predisposition is quantified using the crossing between modeled lifting condensation level (LCL) and convectively grown ABL depth. The LCL-ABL depth crossing is necessary for air saturation but not sufficient for cloud formation and subsequent convective rainfall occurrence. However, such crossing forms the main template for which all subsequent dynamical processes regulating the formation (or suppression) of convective rainfall operate on. If the feedback between surface fluxes and FA conditions is neglected, a reduction in latent heat flux associated with reduced WT levels is shown to enhance the ABL-LCL crossing probability. When the soil-plant system is fully coupled with ABL dynamics thereby allowing feedback with ABL temperature and humidity, FA states remain the leading control on CRP. However, vegetation water stress plays a role in controlling ABL-LCL crossing when the humidity supply by the FA is within an intermediate range of values. When FA humidity supply is low, cloud formation is suppressed independent of surface latent heat flux. Similarly, when FA moisture supply is high, cloud formation can occur independent of surface latent heat flux. In an intermediate regime of FA moisture supply, the surface latent heat flux controlled by soil water availability can supplement (or suppress) the necessary water vapor leading to reduced LCL and subsequent ABL-LCL crossing. It is shown that this intermediate state corresponds to FA values around the mode in observed humidity lapse rates γ_w (between -2.5×10^{-6} and -1.5×10^{-6} kg kg^{-1}m^{-1}), suggesting that vegetation water uptake may be controlling CRP at the study site.

1. Introduction

The interplay between groundwater table (WT) variations, root-zone soil moisture content, land surface fluxes of sensible (H_s) and latent heat (LE), and cloud formation continues to draw significant research attention [e.g., *Koster et al.*, 2004; *Maxwell et al.*, 2007; *Santanello et al.*, 2007; *de Arellano et al.*, 2012; *Katul et al.*, 2012]. In particular, the indirect effects of vegetation on convective rainfall initiation, while essential to a myriad of problems (e.g., weather and climate predictions, water resources management), remain elusive because of the large number of interacting biotic and abiotic processes within the Soil-Plant-Atmosphere (SPA) system. Atmospheric moisture transport and the dynamics of H_s and LE mediated by the SPA system are determinants of diurnal variations of the convective Atmospheric Boundary Layer (ABL) height ($= z_{ABL}$) and of the Lifting Condensation Level (LCL) height ($= z_{LCL}$) as discussed elsewhere [*Siqueira et al.*, 2009]. A crossing of ABL and LCL is only a necessary condition for the occurrence of the thermodynamic state that leads to air saturation and can be interpreted as a prerequisite for the occurrence of convective rainfall [*Juang et al.*, 2007; *Siqueira et al.*, 2009]. Although an ABL-LCL crossing is only necessary and not sufficient, exploring these necessary conditions promoting such crossing is an obvious first step to begin unfolding the role of the SPA system in controlling convective rainfall [*Juang et al.*, 2007; *Siqueira et al.*, 2009] and frames the scope of the work here. Following the ABL-LCL crossing, if parcels of air possess sufficient energy to reach the level of free convection (higher than the LCL), and if the availability of condensation nuclei is such that the liquid film on them grows

to a sufficient size to allow raindrops to reach the land surface without first evaporating, rainfall can occur. These latter processes operate after the ABL-LCL crossing is achieved, and hence the ABL-LCL crossing is the minimum necessary condition required for rainfall occurrence. It is for this reason that the term predisposition to convective rainfall is used here to describe the ABL-LCL crossing when the ABL is growing convectively. The interplay between soil moisture and atmospheric conditions leading to ABL-LCL crossing is explored by means of a simplified model coupling groundwater table fluctuations, soil moisture within the rooting zone, vegetation, and atmospheric dynamics complemented by long-term measurements collected in a Loblolly pine plantation situated in the lower coastal plain of North Carolina, USA. Previous studies considered the effects of soil moisture on boundary layer dynamics [e.g., *Koster et al*., 2004; *Maxwell et al*., 2007], showing that belowground processes can indeed impact rainfall initiation. For example, using large-scale numerical simulations and coupling regional atmospheric models with subsurface soil moisture redistribution schemes but simplified root-plant stomatal representations, *Maxwell et al*. [2007] revealed significant correlations between groundwater level, surface temperature, latent heat flux, and initiation of the first convective cells. Other studies focused instead on Free Atmosphere (FA) feedbacks on rainfall under simplified soil moisture conditions [e.g., *Clark and Arritt*, 1995; *daRocha et al*., 1996; *Findell and Eltahir*, 2003; *Siqueira et al*., 2009; *Konings et al*., 2010]. However, the interplay between water table level and predisposition to rainfall (or crossing of convectively grown ABL and LCL) under different FA conditions continues to resist complete theoretical treatment, and motivates this work. The basic premise (hypothesis H1) is that a deeper WT causes an increase in H_s because of reduced supply of water to the root-plant system (a hypothesis supported by model calculations of *Maxwell et al*. [2007] that show significant correlations between surface temperature and groundwater level). As a consequence, a deepening of the WT leads to an increase in the convective ABL height thereby enhancing the ABL-LCL crossing likelihood. In this work, the WT depth is used as a "control parameter" influencing the root-zone soil moisture conditions. As a matter of fact, while root-zone soil moisture is affected by local scale heterogeneity, WT variations are governed by much larger scale and long-term (much longer than diurnal) land-atmosphere interactions. On the other hand (hypothesis H2), a deeper WT also reduces *LE* (and concomitant water vapor concentration within the ABL) thereby increasing the LCL and reducing the ABL-LCL crossing likelihood. Such reduction of *LE* may be mediated by the FA state if sufficient water vapor is entrained at the upper boundary of the ABL (the ABL top) or enters laterally through moisture transport. Here, the humidity lapse rate is also used as another "control parameter" to define different FA humidity distributions (and consequent entrainment fluxes at the ABL top). It is to be noted that entrainment velocity from the FA is proportional to dz_{ABL}/dt, the time variation of z_{ABL}, and hence is dependent on H_s, where t is time. The coexistence of these two competing effects suggests that all the components of the SPA system are intimately related when soil water and FA water vapor entrainment are the main water sources contributing to saturation and subsequent cloud formation. Within this context, it is reasonable to assume that for a given WT depth, there must exist a minimum threshold value of FA water vapor entrainment below which no rainfall can occur. The objective of this work is to examine the predisposition of the rain/no-rain threshold behavior by testing the two hypotheses mentioned above via a combined use of model runs and field measurements. The aim is to explore only necessary conditions in terms of water table and FA states promoting the ABL-LCL crossing in the system to be studied. The WT (impacted by long-term hydrological conditions) and FA (impacted by large-scale weather pattern) states that shift the system to a crossing/noncrossing condition define the boundary conditions on the rainfall/no rainfall threshold. It is to be noted that the work here is not intended to explore land-surface fluxes and their effect on cloud formation, cloud microphysics, and rainfall amounts. Such explorations have been extensively studied and are described elsewhere [e.g., *Gentine et al*., 2013a]. Rather, the focus is on how a limited availability in one of the two main sources of water (WT and FA) to the SPA system impacts the predisposition to convective rain and the rain/no-rain threshold. An immediate application of these explorations is whether large-scale reductions in WT height can be partly mitigated by increased probability of rainfall occurrences through a land-atmosphere feedback mechanism. This feedback mechanism may reveal hydrological states (via WT) and weather patterns (via FA) promoting limited self-regulation within the hydrological cycle. Moreover, this work features the role of vegetation (local in spatial scale) and free atmospheric states (regional in spatial scale) in regulating soil-atmosphere feedback mechanisms that assist in delineating the deterministic component of rainfall formation (ABL-LCL crossing). In fact, while a strong coupling between soil moisture and precipitation has been demonstrated in some regions around the globe [*Koster et al*., 2004], the nature of these feedbacks remains elusive because the simultaneous roles of groundwater table changes and free atmospheric states have not been unfolded.

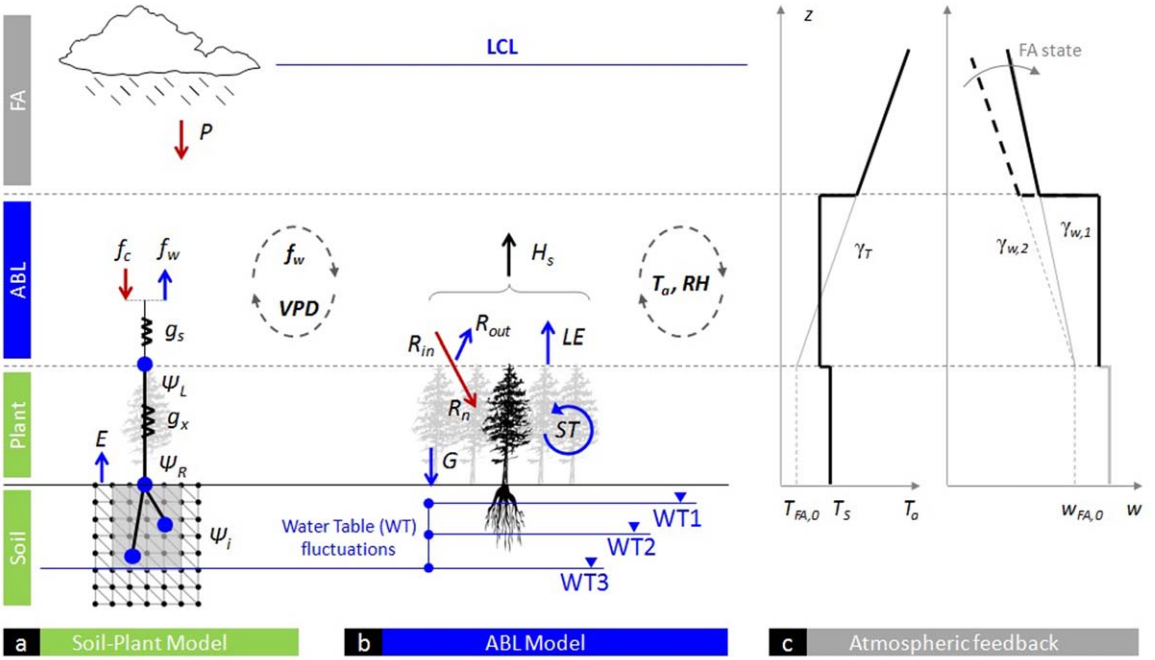

Figure 1. Conceptual Model: (a) The soil-plant system is modeled in terms of water potential in the soil (ψ_i), plant trunk (ψ_R), and plant leaf (ψ_L) through a series of conductance (e.g., trunk xylem, g_x, and stomata, g_s). The Soil-Plant model is linked to the atmosphere by transpiration flux f_w, carbon assimilation f_c and VPD. The ABL model is based on (b) a 1-D energy balance and (c) the atmospheric feedback is included by considering the evolution of ABL temperature (T_a) and humidity (w).

2. Mathematical Methods

A conceptual model of the SPA system is illustrated in Figure 1. The modeling approach is briefly presented here. Further details on the soil-plant model implementation and the parameters used in the model runs are presented elsewhere [*Manoli et al.*, 2014]. For the purposes here, a well-mixed ABL representation is assumed in which water transport and humidity gradients within the ABL are not explicitly modeled. However, the z_{ABL} and z_{LCL} dynamics are explicitly linked to variations in H_s and LE and prescribed FA states. Moreover, it is assumed that the FA states evolve on time scales much longer than those associated with dynamics of H_s and LE, so that during the course of a single day the FA states can be treated as constants not impacted by diurnal variations in local H_s and LE. However, over the course of several days the FA states can be altered. While this is a simplified representation for z_{ABL} and z_{LCL} dynamics and FA states, it allows the exploration of soil-atmosphere interactions as mediated by root water uptake (see Figure 1) without requiring all aspects of the meso-scale dynamics occurring above the ABL to be resolved. A list of all model variables, abbreviations, and parameters is provided in the supporting information.

2.1. The Soil-Plant Model

In the model representation here, water flow through the SPA system (Figure 1a) is dictated by water potential gradients between the soil (ψ), the plant trunk (ψ_R), and the leaf (ψ_L) and by a network of conductivities that vary nonlinearly with the local value of the water potential in each level [*Volpe et al.*, 2013; *Manoli et al.*, 2014]. Soil moisture dynamics are described using a 3-D Richards' equation modified to include a 3-D macroscopic root water uptake (RWU) sink:

$$S_s S_w \frac{\partial \psi}{\partial t} + \phi \frac{\partial S_w}{\partial t} = \vec{\nabla} \cdot \left[\mathbf{K}_s K_r \left(\vec{\nabla} \psi + \eta_z \right) \right] + q(\psi, x, y, z, t, \psi_L), \quad (1)$$

where S_s is the elastic storage term (m^{-1}), S_w is water saturation, ψ is water pressure head in the soil (m), t is as before time (s), ϕ is porosity, $\mathbf{K}_s$ is the saturated hydraulic conductivity ($m\ s^{-1}$) tensor, K_r is the relative hydraulic conductivity, $\eta_z = (0,0,1)^T$, z is the vertical coordinate directed upward and q is a local source/sink term (s^{-1}) within the root-zone used to couple soil water dynamics with the root-plant-atmosphere continuum via the leaf water potential ψ_L. The pressure head dependencies in the general storage term and relative

hydraulic conductivity in equation (1) are represented using the characteristic relations (water retention curves) proposed by *van Genuchten and Nielsen* [1985]. Equation (1) is solved numerically using the CATHY model (CATchment Hydrology) [*Camporese et al.*, 2010], a linear tetrahedral finite element code based on a backward Euler scheme and Newton-like iterations [*Paniconi and Putti*, 1994]. Discretization of the source term is obtained by means of a second-order accurate midpoint rule by which at each grid node *i* the source term $q_i = q(\psi_i, x_i, y_i, z_i, t, \psi_L)$ is multiplied by the corresponding nodal volume V_i. The flux per unit volume, accounting for the uptake of soil water by roots in grid node *i*, is defined as [*Manoli et al.*, 2014]:

$$q_i = -g_i \cdot [(\psi_R + z_R) - (\psi_i + z_i)] a_{R,i}, \tag{2}$$

where z_R (m) is the vertical coordinate of the plant (at the base of the trunk), $a_{R,i} = 2\pi r_r B_i$ is the root surface area per unit soil volume, r_r is the effective root radius responsible for water uptake (assumed to be 2 mm commensurate with expectations for fine roots) and B_i the root length density, z_i (m) is the vertical coordinate referring to the *i*th node, ψ_R and ψ_i the water potential (m) in the xylem and in the soil (*i*th grid node), respectively. The root-soil conductance g_i (s^{-1}) is computed as the series of soil and root conductances described elsewhere [*Siqueira et al.*, 2008; *Volpe et al.*, 2013; *Manoli et al.*, 2014].

The water potential in the xylem, ψ_R, is computed as a function of the water potential in the leaf, ψ_L (m), by imposing $\sum_i q_i \cdot V_i = f_w$, where V_i is the volume (m^3) referred to the *i*th node and f_w is the transpiration rate ($m^3\ s^{-1}$) from the plant, calculated as:

$$f_w = -g_x \cdot V_x \frac{[(\psi_L + z_L) - (\psi_R + z_R)]}{h_c}, \tag{3}$$

where g_x is the xylem conductance (s^{-1}), $h_c = z_L - z_R$ is the mean canopy height (m) and $V_x = A_x \cdot h_c$ is the xylem volume (m^3), being A_x the xylem area. To ensure continuity in the soil-plant-atmosphere system, the transpiration from the plant (equation (3)) is set to be identical to the mass transfer of water vapor between the leaf and the atmosphere (i.e., no capacitance), so that f_w can also be expressed as:

$$f_w = a \cdot g_s(\psi_L) \cdot VPD \cdot \epsilon_w \cdot LAI \cdot A_c, \tag{4}$$

where $a = 1.6$ is the relative molecular diffusivity of water vapor with respect to CO_2, A_c is the canopy area (m^2), g_s is the stomatal conductance (mol $m^{-2}s^{-1}$) for carbon dioxide, *VPD* is the vapor pressure deficit (mol/mol) and $\epsilon_w = M_w/\rho_w$, being M_w and ρ_w molar weight (g mol^{-1}) and density (kg m^{-3}) of water, respectively. The stomatal conductance g_s is determined so as to maximize carbon gain subject to water availability according to *Katul et al.* [2010].

Coupling equation (3) with equation (4) provides a nonlinear closure equation for the calculation of the unknown ψ_L. This combined root-xylem-leaf formulation is shown to reproduce the many features of the soil-plant system including soil moisture dynamics, hydraulic redistribution, stomatal shutdown at midday, branch-scale water potentials, transpiration, and carbon assimilation fluxes [*Volpe et al.*, 2013; *Manoli et al.*, 2014]. The main lower boundary condition on the soil-plant model is the water table level and the coupling with an atmospheric model allows a full description of the land-atmosphere feedback mechanisms.

2.2. The ABL Model

2.2.1. Dynamics of ABL and LCL Heights

The LCL height z_{LCL} is determined from commonly used expressions [*Stull*, 1988; *Juang et al.*, 2007]

$$z_{LCL} = \frac{RT_a}{gM_a} \cdot ln\left(\frac{P_s}{P_{LCL}}\right), \tag{5}$$

where $R = 8.314$ (J $mol^{-1}\ K^{-1}$) is the universal gas constant, T_a is the mean air temperature (K), g is the gravitational acceleration (m s^{-2}), M_a is the molecular weight of air ($\sim$ 29 g mol^{-1}), P_s (kPa) is the atmospheric pressure at the canopy surface, and P_{LCL} (kPa) is the atmospheric pressure at z_{LCL}. The value of P_{LCL} can be expressed as [*Stull*, 1988; *Juang et al.*, 2007]:

$$P_{LCL} = P_s \left(\frac{T_{LCL}}{T_a}\right)^{3.5}, \tag{6}$$

where T_{LCL} (K) is the saturation point temperature at z_{LCL}, which can be derived from the Clausius-Clapeyron equation [*Stull*, 1988; *Juang et al.*, 2007]:

$$T_{LCL} = \frac{2840}{3.5 \cdot ln(T_a) - ln\left(\frac{rP_s}{0.622+r}\right) - 7.108} + 55, \tag{7}$$

where the value 3.5 represents the inverse of the Poisson constant for air. Parameter r is the near-surface atmospheric water vapor mixing ratio, determined as [*Wallace and Hobbs*, 2006]:

$$r = 0.622 \cdot \frac{e_a(T_a)}{P_s - e_a(T_a)}, \tag{8}$$

where the actual vapor pressure e_a (kPa) is computed from $e_a = e_s \cdot RH/100$, RH (%) is the air relative humidity and e_s (kPa) is the saturation vapor pressure, given by the Clausius-Clapeyron relation:

$$e_s(T) = 0.6108 \cdot \exp\left(\frac{17.27 \cdot (T - 273.15)}{(T - 273.15) + 237.3}\right), \tag{9}$$

where T (K) is the atmospheric temperature. Using an "encroachment hypothesis," the dynamics of the ABL height z_{ABL} is defined as [*Stull*, 1988]:

$$\frac{dz_{ABL}}{dt} = \frac{H_s \cdot (1+\beta)}{\gamma_T \cdot z_{ABL}} \tag{10}$$

where γ_T is the temperature lapse rate (estimated using a linear regression analysis from sounding data at 5 K km^{-1} (Morehead/Newport Airport, MHX) during the summer season of 2007 when convective rainfall dominates much of the precipitation regime, i.e., June–September, at Morehead/Newport Airport using a linear regression analysis) and H_s is the surface sensible heat flux (described later). According to *Tennekes* [1973], the sensible heat flux entrained from the top of the mixed layer may be treated as a constant fraction β of H_s. Numerical and experimental studies [*Betts et al*., 1992; *Kim and Entekhabi*, 1998] suggest that β varies between 0.2 and 0.4. Such zeroth-order jump models are effective at describing the dynamics of the boundary layer states as suggested by direct comparisons to Large Eddy Simulation (LES) runs described elsewhere [*Pino et al*., 2006]. The utility and skill of such slab models in predicting the formation of shallow cumuli are reviewed elsewhere [*Gentine et al*., 2013b].

2.2.1.1. Energy Balance

The sensible heat flux H_s (K m s^{-1}) is determined as a residual from the energy balance at the canopy top:

$$H_s(T_s) = \frac{1}{c_p \cdot \rho_a}\left[R_n(T_s) - LE - G - ST\right], \tag{11}$$

where T_s (K) is the canopy skin temperature, $LE = \lambda_v \cdot \rho_w \cdot f_w \cdot A_c^{-1}$ is the latent heat flux (W m^{-2}) with $\lambda_v = 44{,}000$ J mol^{-1} being the latent heat of vaporization, $c_p = 1005$ J kg^{-1} K^{-1} is the specific heat capacity of dry air at constant pressure, ρ_a and ρ_w (kg m^{-3}) are the air and water density, respectively. The value of the soil heat flux G (W m^{-2}) is estimated from field data. Storage of heat within the canopy volume ST (W m^{-2}) is assumed to be 5% of the net radiation R_n during daytime conditions. This value can be justified as follows. The canopy storage ST_c is of the same order of magnitude of the air heat storage ST_a [*Meyers and Hollinger*, 2004; *Garai et al*., 2010], which can be computed over a 30 min period τ for a 1 degree warming ΔT_a (typical of midday) as $ST_a = (\rho_a \cdot c_p \cdot \Delta T_a \cdot h_c)/\tau \sim 12$ W/m^2. The entire storage term within the canopy is then given by the sum of the canopy material and the air storage, $ST = ST_c + ST_a \sim 24$ W/m^2, i.e., $\sim 5\%$ of the net radiation (given $R_n \sim 500$ W/m^2 during midday). The net radiation R_n (W m^{-2}) is determined as $R_n = R_{ns} - R_{nl}$, where R_{ns} and R_{nl} are the net shortwave and longwave radiation at the canopy top, respectively. The net shortwave radiation is calculated as

$$R_{ns} = (1-\alpha) \cdot R_s, \tag{12}$$

R_s being the incoming shortwave radiation measured above the canopy and α the canopy albedo. The net longwave radiation is calculated according to the Stefan-Boltzmann's law:

$$R_{nl}(T_s) = \sigma\left[\varepsilon_s T_s^4 - \varepsilon_a T_a^4\right], \tag{13}$$

where $\sigma = 5.67 \cdot 10^{-8}$ (W K^{-4} m^{-2}) is the Stefan-Boltzmann constant and ε_s is the canopy surface emissivity that varies between 0.8 and 1.0 [*Garratt and Brost*, 1981]. It is assumed here that $\varepsilon_s = 0.9$, as commonly

done in many other models [*Sobrino et al.*, 2005]. The emissivity of the clear-sky atmosphere ε_a is determined from [*Brutsaert*, 1975]:

$$\varepsilon_a = 1.24 \cdot \left(\frac{e_s(T_a) \cdot \frac{RH}{100}}{T_a} \right)^{\frac{1}{7}}. \tag{14}$$

This formulation was shown to be reasonably accurate near the ground when compared to other detailed formulations even for nocturnal conditions, where incident longwave radiation represents the entire radiative load [*Siqueira and Katul*, 2010].

2.2.1.2. Aerodynamic Balance

The sensible heat flux between the canopy surface and the atmosphere can be expressed as:

$$H_s(T_s) = g_a(T_s - T_a) \tag{15}$$

where $g_a = 1/r_a$, with r_a (s/m) being the aerodynamic resistance, calculated as [*Allen et al.*, 1998]:

$$r_a = \frac{ln\left[\frac{z_m - d}{z_{om}}\right] \cdot ln\left[\frac{z_h - d}{z_{oh}}\right]}{k^2 \cdot u_z} \tag{16}$$

where z_m is the height of wind speed measurement (m), z_h is the height of the temperature measurement (m), $d = 2/3\ h_c$ is the zero-plane displacement height (m) for the flow valid for dense canopies, $z_{om} = 0.123\ h_c$ is the roughness length governing momentum transfer (m), $z_{oh} \approx 0.1\ z_{om}$ is the roughness length governing transfer of heat and vapor (m), $k = 0.41$ is the von Kármán constant and u_z is the wind speed (m/s) at height z_m above the ground.

2.2.1.3. Nonlinear Closure Equation

Equating equation (11) and equation (15) provides a nonlinear equation for the unknown T_s:

$$H(T_s) = g_a \cdot (T_s - T_a) - \frac{1}{c_p \cdot \rho_a} \cdot [R_n(T_s) - LE - G - ST] = 0, \tag{17}$$

which can be solved iteratively by the Newton-Raphson method. Equation (17) is a fourth-order polynomial with four real solutions. To ensure the convergence of the numerical procedure to a correct value of T_s, the air temperature T_a is used as initial guess of the Newton iteration (i.e., $T_s(0) = T_a$). Equation (10) is solved numerically by a forward Euler scheme. As the simulations require a continuous ABL height, a Nocturnal Boundary Layer (NBL) must also be included initially. A stationary NBL height $z_{night} = 100$ m is imposed [*Garratt and Brost*, 1981; *Siqueira et al.*, 2009]. This height is constant as long as nocturnal conditions prevail and only serves to initialize daytime ABL model calculations. The transition from day-to-night is also abrupt, with the ABL height dropping from its near maximum value to z_{night} when sensible heat flux at the surfaces switches from being positive to negative.

2.2.2. Soil-Plant-ABL Coupling

The Soil-Plant model is coupled with the atmosphere via the stomatal conductance g_s [*Katul et al.*, 2010; *Manoli et al.*, 2014]:

$$g_s(\psi_L) = \frac{a_1}{a_2 + s\, c_a} \left[-1 + \left(\frac{c_a}{a\, \lambda(\psi_L)\, VPD} \right)^{1/2} \right] + g_{s,n} \tag{18}$$

where a_1 and a_2 are photosynthetic parameters that vary depending on whether light or Rubisco limits photosynthesis, s is a model constant reflecting long-term ratio of intercellular to ambient atmospheric c_a, c_a (mmol mol^{-1}) is the CO_2 concentration in the atmosphere and the cost parameter λ (μmol mol^{-1}) is interpreted as the cost of water in carbon units for the plant to complete photosynthesis. It is estimated from the time-integrated leaf water potential according to [*Manzoni et al.*, 2011]. The nocturnal stomatal conductance $g_{s,n}$ is determined from the relation between sapflow and *VPD* [*Manoli et al.*, 2014]. Given the

canopy temperature T_s, it is possible to define the vapor pressure deficit (*VPD*) as a function of leaf vapor pressure and vapor pressure at ambient conditions:

$$VPD = e_s(T_s) - e_s(T_a) \cdot \frac{RH}{100} \tag{19}$$

The soil-plant-atmosphere continuum is thus fully coupled.

2.3. Atmospheric Feedback

To describe the simultaneous effects of surface fluxes and FA conditions on ABL and LCL dynamics, a well-mixed ABL is assumed and the conservation equations for ABL potential temperature T_a and specific humidity w are employed as follows [*Porporato*, 2009]:

$$z_{ABL}\frac{dT_a}{dt} = H_s + (T_{FA} - T_a) \cdot \frac{dz_{ABL}}{dt} \tag{20}$$

$$z_{ABL}\frac{dw}{dt} = \frac{LE}{\rho_a \lambda} + (w_{FA} - w) \cdot \frac{dz_{ABL}}{dt} \tag{21}$$

where T_{FA} and w_{FA} are the potential temperature and humidity in the FA above z_{ABL}. Following *Porporato* [2009], a linear profile of T_{FA} and w_{FA} in the free atmosphere are assumed from which it directly follows that:

$$T_{FA} = T_{FA,0} + \gamma_T \cdot z_{ABL} \tag{22}$$

$$w_{FA} = w_{FA,0} + \gamma_w \cdot z_{ABL} \tag{23}$$

where $T_{FA,0} = 288$ (K) and $w_{FA,0} = 7.58 \times 10^{-3}$ (kg kg^{-1}) according to *Porporato* [2009]. Relative humidity in percent is calculated as $RH = 100 \cdot w/w_s$, where $w_s = 0.622 \cdot e_s(T_a)/(P_s - e_s(T_a))$ is the specific humidity at saturation (kg kg^{-1}). Modeled T_a and RH are then coupled with the previously described SPA model, thus providing a fully coupled description of the ABL-FA structure.

3. Numerical Experiments

To evaluate the model's ability in capturing predisposition of the SPA system to convective cloud formation, the modeling framework is tested against field measurements from a Loblolly pine plantation in North Carolina (labeled Simulation S0). The parameterized model is then used to investigate hypotheses H1 and H2 (see Section 1) by performing two additional sets of numerical experiments, labeled as S1 and S2. The first set (S1) pins the dynamics of LCL to observed RH and T_a. Hence, the S1 setup excludes any possible feedback from the SPA system on ABL states that impact the dynamics of the LCL. The second set (S2) explores the behavior of the system when the SPA model is allowed to alter ABL dynamics, RH and T_a as discussed earlier in the model description. It is to be noted that the focus here is not on the prediction of rainfall initiation or amounts, but on the predisposition as quantified by the ABL-LCL crossing (i.e., saturation). The connection between land surface to FA states require a full-fledged regional atmospheric model and is beyond the scope here.

3.1. Study Site

The model is applied to a site where (i) the rooting system is sufficiently deep to avoid water stress, (ii) the WT variations are large, and (iii) the summertime rainfall is primarily convective. The site is a Loblolly pine (*Pinus taeda L.*) plantation situated in the lower coastal plain of North Carolina, USA (US-NC2 in the Ameriflux database). Briefly, this site is located at 35°48′N, 76°40′W within the outer coastal plain mixed forest province of North Carolina in the southeastern U.S. [*Sun et al.*, 2010]. This Loblolly pine stand is a midrotation plantation owned and operated by Weyerhaeuser Company and was established in 1992 after clear-cutting the previous mature pine plantation. The histic-mineral soil at this site is classified as Belhaven series. The watersheds are drained with a network of parallel ditches (90 cm–130 cm deep; 90 m spacing) and more widely spaced roadside channels. Drainage lowers the water table height, improving site access (management) and tree productivity by reducing stresses caused by excessive soil water conditions during winter months. The long-term (1945–2010) average annual precipitation is 1308 ± 201 mm, evenly distributed throughout the year. Long-term mean annual temperature averaged 15.5°C, with a monthly high occurring in July (26.6°C), and a monthly low occurring in January (6.4°C). The following

micrometeorological parameters were measured above canopy: air temperature (T_a, HMP45AC, Vaisala, Finland), photosynthetically active radiation (*PAR*, LI-190, Licor Inc.), net radiation (R_n, CNR-1, Kipp & Zonen, Delft, the Netherlands) and precipitation (*P*, TE-525, Campbell Scientific Inc., (CSI), Logan, UT, USA). The *PAR* measurements were corrected for sensor drift based on annual comparisons against an Ameriflux standard sensor (PARLITE, Kipp & Zonen) assuming linear drift. Canopy latent heat (*LE*) flux was measured using open-path eddy covariance system and the data were processed as reported previously [*Noormets et al*., 2010; *Domec et al*., 2012]. Soil heat flux was measured at three locations using heat flux plates (model HFT3, CSI, Logan, UT, USA) buried 5 cm below the ground surface. Soil heat flux measurements were affected by uncertainty due to spatial heterogeneity and temporal integration within a half-hourly period. However, as is the case for dense forested canopies where a significant portion of the incident radiation above the canopy is intercepted by the canopy before arriving to the forest floor, *G* is a small component of the energy balance [*Sun et al*., 2010]. Hence, the overall accuracy of model predictions are not significantly affected by the treatment of *G*. All the micrometeorological, hydrological, and flux measurements are presented as daily means (or sums) over a a 30 min interval. Gaps in 30 min *LE* data amounted to 7 and 14% for 2007 and 2008, respectively and were "filled" using empirical monthly correlations between observed *ET* and FAO potential evapotranspiration (*PET*) [*Noormets et al*., 2010; *Domec et al*., 2012; *Aubinet et al*., 2012; *Novick et al*., 2009]. The choice of a 30 min interval is conventionally viewed as a compromise between (i) the need to sample over a sufficiently long duration so as to resolve the main low-frequency contributions to the cospectra of turbulent fluxes (whose frequency integration results in measured *LE* and H_s), (ii) the requirements for ensuring stationary conditions so as to interpret measured fluxes above the canopy as depth integrated sources and sinks within the soil-plant system, and (iii) the need to resolve diurnal variations in sensible heat flux so as to delineate in time the LCL-ABL crossing. A number of studies have suggested that in a convective dominated ABL, the 30 min duration may be suppressing low-frequency contributions to measured *LE* and H_s leading to their underestimation [see e.g., *Foken*, 2008].

3.2. Model Evaluation (Simulation S0)

The SPA model was parametrized for the pine plantation case study site (Simulations S0) using data collected in 2007–2008 described elsewhere [*Sun et al*., 2010]. The starting point here is the 3-D soil-plant model calibrated by *Manoli et al*. [2014] based on data from the same site. Next, the measured albedo from the CNR-1 radiometer is "fine-tuned" (i.e., from measured incident and reflected shortwave radiation) and the parameter β of equation (10) is calibrated to capture the dynamics of sensible and latent heat fluxes and net short and long wave radiations. The 3-D model of *Manoli et al*. [2014] was reduced to a 1-D mode by planar averaging. The computational domain (5 m $\times$ 5m $\times$ 5 m) is composed of a vertical mesh where Richards' equation is solved, surrounded by nodes where the Boundary Conditions (BCs) are imposed. The bottom of the soil domain has a no-flow BC, while in the lateral nodes the WT depth is specified according to the site observations by imposing no-flux in the nodes above the WT and hydrostatic BCs below the WT. The surface nodes are subjected to the sequence of rainfall and understory evapotranspiration as measured at the site [*Manoli et al*., 2014]. The central node corresponds to the plant trunk base. Air temperature, photosynthetically active radiation (PAR), relative humidity, and incoming shortwave radiation were imposed as atmospheric forcing on a 30 min interval.

3.3. Synthetic Simulations

In these simulation runs, the same model setup is used but different WT BCs are imposed. Moreover, understory evapotranspiration and rainfall are turned off.

3.3.1. Simulation S1

Simulation S1 measured T_a and *RH* time series (years 2007–2008) near the surface are assigned as model input, effectively prescribing the z_{LCL} variations in time. In this case, only the effects of the ABL dynamics on the predisposition to convective rainfall are allowed and modeled. That is, while H_s and *LE* are computed on the basis of imposed T_a and *RH* values, the latter are not dynamically recomputed in the course of the simulation and are simply imposed based on tower observations. A constant WT depth is set during each 2 year period simulation and 8 different simulations are run, in which the WT depth is uniformly varied in the range 0.5–4 m below the surface (mbs) to cover both wet and dry soil moisture states. This choice of BCs is justified as variations in WT occur on time scales much longer than the diurnal variations over which ABL-LCL crossings occurs as earlier noted. The variations of WT depth represent varying water availability, and

the corresponding model results may be also thought of as representative of the effects of varying soil water saturation in the root zone. In general, while soil moisture measurements are typically pointwise, WT fluctuations represent integrated hydrological conditions at much larger scales and are therefore more appropriate to summarize land-atmosphere interactions. However, space-time variations of soil moisture bounded by WT and the soil-atmosphere interface are fully captured by the model including all macroscopic variations in root-water uptake patterns. The results described next, while focused on the study site, do have wider implications for root-mediated controls of storm intensity and interarrival rates—especially how they feedback to convective rainfall predisposition.

3.3.2. Simulation S2

The second set of model runs (S2) is a fully coupled numerical experiment that considers the simultaneous effects of H_s, LE and FA conditions on z_{ABL} and z_{LCL} dynamics. In these model runs, the depth-averaged T_a and RH within the ABL are dynamically computed based on the state of the system (equations (20) and (21)). Simulation runs are conducted for a 100 days period with periodically forced atmospheric conditions (i.e., PAR and incoming shortwave radiation) collected on a typical clear sky summer day (arbitrarily chosen here as 2 September, 2007 because no clouds were detected in the radiation measurements and the maximum measured clear-sky shortwave radiation is close to its theoretical maximum at this latitude and site elevation). In particular, the periodicity of the atmospheric conditions is set to 24 h, meaning that the diurnal variation in PAR and incoming radiation is set identical every day throughout the simulation period. In S2, 100 day simulation runs with daily repeating diurnal BCs are used to achieve a stationary state at which the predisposition to rainfall is then evaluated using the ABL-LCL crossings. Since nocturnal ABL dynamics are not modeled, measured T_a and w (DOY 245) were imposed at night (periodically forced each evening) and only daytime ABL dynamics are explicitly modeled. The whole scheme is then repeated to explore all the different combinations of WT depth and w_{FA}, obtained by varying γ_w in the range of values observed at the site (-5×10^{-6} and -0.5×10^{-6} kg kg^{-1} m^{-1}).

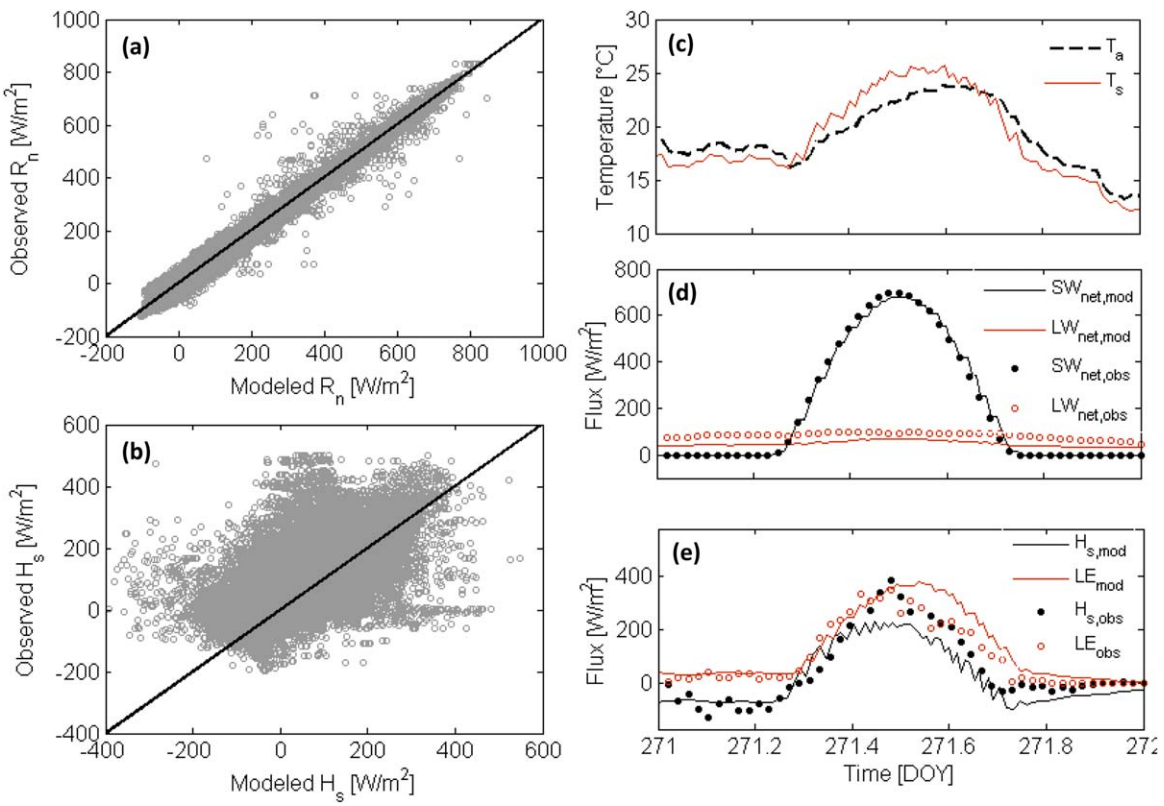

Figure 2. Model performance (S0): Comparison between modeled and measured (30 min data, years 2007–2008) (a) net radiation and (b) sensible heat flux. Diurnal variation of measured mean air and modeled (c) canopy temperature, (d) net short and long wave radiation, (e) sensible heat and latent heat fluxes are shown (DOY 271, year 2007) and compared with measurements.

4. Results and Discussion

4.1. Model Evaluation (Simulation S0)

Following calibration, the agreement between model results and measurements is acceptable (Figure 2). In particular, measured and modeled R_n are matched with a correlation coefficient $r = 0.99$, a regression slope $s_r = 0.99$ and intercept $b_r = -6.0$ W m^{-2} commensurate with the net radiometer sensor resolution (Figure 2a). Figure 2d shows good agreement between observed and modeled *LW* and *SW* radiation. While the latter is to be expected because of the fine-tuning of the albedo, the former is entirely a model result. The dynamics of measured T_a and modeled T_s, shown in Figure 2c, are realistic and in agreement with expected patterns. Some discrepancies exist between modeled and eddy-covariance measured H_s and *LE* (Figure 2e). In particular, despite the small H_s values at this site relative to R_n, H_s is matched with $r = 0.68$, $s_r = 0.75$ and $b_r = 30.6$ W m^{-2} (Figure 2b). The model results overestimated eddy-covariance measured *LE*, especially for the afternoon runs, where the ABL height is near its maximum and where measured fluxes by the eddy-covariance system are likely to be underestimated due to censoring of large-scale eddy motion contribution in a 30 min interval as well as entrainment effects. Interestingly, the measured energy balance closure here (estimated within 30–50 W m^{-2} in *Sun et al.* [2010]) is more prevalent in the afternoon and its magnitude appears to be commensurate with the *LE* model overestimation of the eddy-covariance measurements. This finding is consistent with the rationale that a 30 min averaging period may lead to an under-estimation of eddy-covariance measurements when z_{ABL} is large. This bias has been documented at other sites [*Stoy et al.*, 2006], where the energy balance closure was shown to increase with increasing atmospheric stability conditions (i.e., from near-neutral to near-convective).

Quite significant for the objectives of this work is the ability of the model to capture the time variation of z_{ABL} (Figure 3) and to predict the timing of rainfall events (Figures 4a and 4b). As already mentioned, the probability of initiation of a rainfall event is necessarily dictated by a crossing of the ABL with the LCL (an example is provided in Figure 4a). Since the LCL height is the minimum height that must be exceeded by buoyant air parcels for condensation to occur, a necessary condition for rainfall generation, it is reasonable to compare modeled ABL-LCL crossing time against observed rainfall occurrences. In this comparison, all

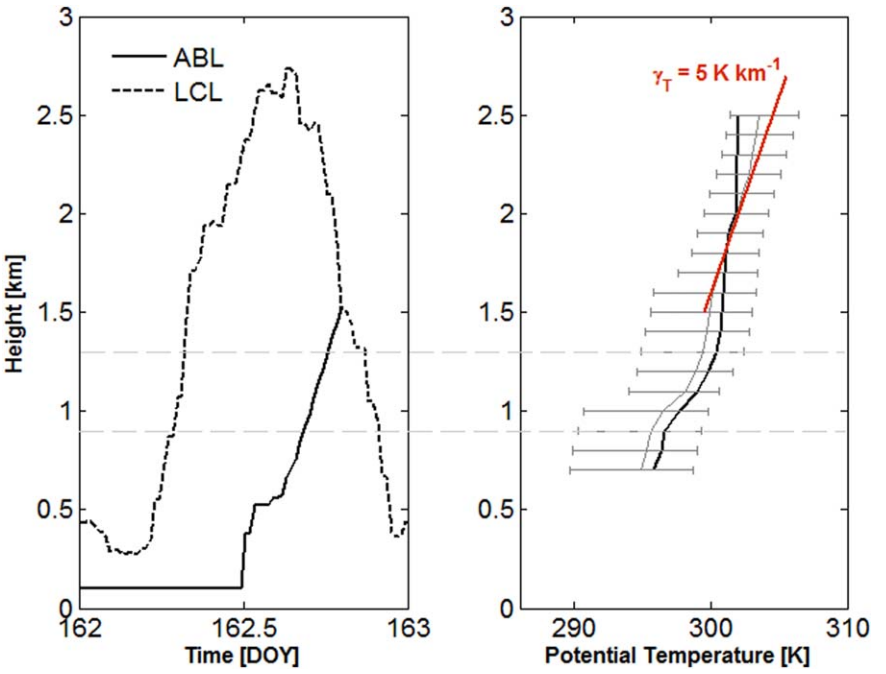

Figure 3. (left) Modeled variations of ABL and LCL heights during DOY 162, year 2007 (Simulation S0); (right) ensemble-averaged (gray line) potential temperature profile and errors from soundings at MHX airport (when a clear boundary layer during June 2007 was identified), potential temperature profile on DOY 162 (black line). The jump in potential temperature observed in the right figure represents the approximate ABL height. In the right figure, the temperature lapse rate above the ABL used in the simulations (red line) is also shown for comparison.

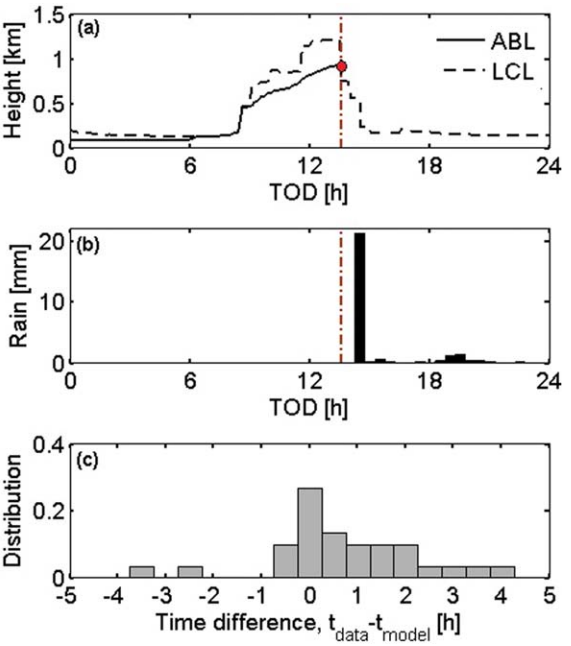

Figure 4. Simulation S0: (a) modeled ABL and LCL heights and their crossing interpreted here as predisposition to rainfall, predicted rainfall event timing (ABL-LCL crossing defined by the red dot in (Figure 4a) and (b) corresponding measured occurrence and amount of precipitation (half-hourly data) on day 191 of year 2007. (c) The probability density function of the time difference between measured convective rainfall events and the ABL-LCL crossings. Note the expected positive skewness in the timing error. In these comparisons all nighttime events and nonclear sky conditions are removed from the measured rainfall time series.

nighttime events and nonclear sky conditions are removed from the measured rainfall time series. Nighttime events are removed because the NBL dynamics are not modeled and are not connected to convective rainfall. Nonclear sky conditions are also neglected to avoid the influence of regional scale phenomena that laterally advect water vapor into the system and are not considered in the slab model. Note that the clear-sky conditions are only invoked prior to the ABL-LCL crossing period. In fact, after their crossing clouds can form, but beyond the crossing point the dynamics of the ABL and LCL are no longer tracked because the predisposition requirement has been satisfied. For this reason, after the crossing occurs, z_{ABL} is set equal to z_{LCL} in the model calculations (see Figures 3 and 4). The probability density function (pdf) of the predicted timing error of rainfall events, defined as the difference between observed rainfall and predicted ABL-LCL crossings $t_{data} - t_{model}$, is positively skewed (Figure 4c), indicating that the model tends to anticipate the timing when rainfall events do occur. This is indeed to be expected, as the ABL-LCL crossing is only a precursor for rainfall occurrences. A period ranging from few minutes up to 2 h following ABL-LCL intersection may be needed for convective rainfall to be realized at the ground if such predisposition to rainfall is actually materialized [*Juang et al.*, 2007]. It is to be noted that modeled crossing events that do not correspond to observed rainfall occurrences were not included in the computation of the probability of timing error. However, they may be used as an index for rainfall generation efficiency as they capture a ratio of predisposed to actual recorded rainfall events.

4.2. Simulation S1: Influence of Water Table Fluctuations

The results from the S1 simulations are illustrated in Figure 5: a first simulation with WT depth set to 0.5 m is used as reference and the transition of the system to different levels of rainfall predisposition for varying WT depths is evaluated by considering the change in the number of ABL-LCL crossings (N_{cross}) observed during the simulation period relative to the reference simulation. Simulation results demonstrate that when the WT depth is increased the frequency of ABL-LCL crossings increases. This increase is to be expected and is due to a decrease in *LE*, corresponding to an increase of H_s (via the energy balance) thereby increasing z_{ABL} (via the ABL budget equation). In fact, N_{cross} increases by more than 20%, following a logical progression. When vegetation is well watered, the WT has no effects on ABL-LCL crossings (Case WT1 in Figure 5). Overall, the progressive lowering of the WT below the root zone (cases WT2 and WT3 in Figure 5) shows that increased plant water stress corresponds to increased buoyancy production of turbulent kinetic energy resulting in higher ABL if no feedbacks on the ABL states are considered. It is to be noted that S1 model results are based on the assumption that *RH* and T_a are externally imposed using measurements and are not affected by H_s and *LE* or ABL dynamics. It is known that a decrease in *LE* can lead to a suppression of ABL clouds [*de Arellano et al.*, 2012] but, on the other hand, it has also been demonstrated that precipitation may actually be initially enhanced (e.g., as observed during the early phases of deforestation in Amazonia [*Chagnon and Bras*, 2005]). The predisposition to rainfall in the actual, fully

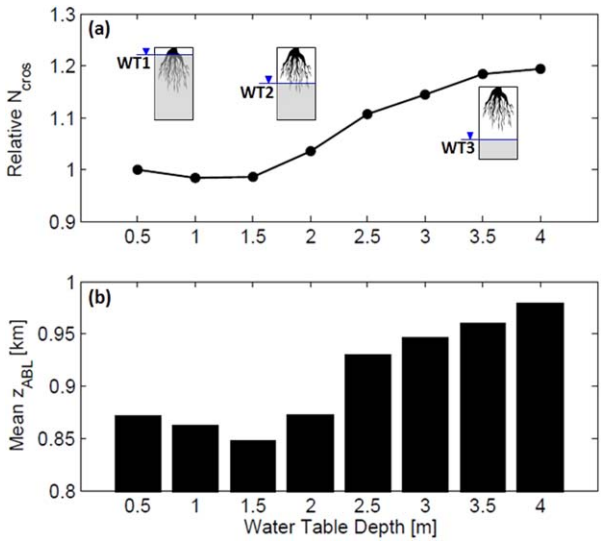

Figure 5. Simulations S1: (a) The effect of increased water table depth on rainfall predisposition determined from the number of ABL-LCL crossings during the simulation period (June–September, 2007–2008). (b) The average value of the ABL height in the different simulations.

coupled, dynamics, is controlled by the interplay between H_s and LE at the land surface and FA conditions at the top of the ABL, considered in the next set of simulations (S2).

4.3. Simulation S2: Atmosphere Feedback

Simulations S2 consider the full coupling between SPA fluxes, ABL T_a and RH, z_{ABL} and z_{LCL}. The ability of the model to capture T_a and RH dynamics during the day here assumed as a reference is illustrated in Figures 6a and 6b, where modeled and measured T_a and RH are compared. Figures 6c–6f show the results of a simulation with WT depth set at 2.5 mbs and a γ_w equal to -2.5×10^{-6} kg kg^{-1} m^{-1} in terms of SPA fluxes, ABL T_a and RH, z_{ABL} and z_{LCL}, for a window centered in the 100 days simulation period. Figure 6f shows ABL-LCL crossings occurring before stationary conditions are reached, and cannot be considered as real crossings. The occurrence of the ABL-LCL crossing is here evaluated only under stationary conditions, i.e., at the end of the 100 day simulation period when day-to-day variations of ABL height become negligible. When the atmospheric feedback between the soil-plant-ABL system and the ABL T_a and RH is allowed, a more nuanced picture emerges (Figure 7). If T_a and RH are entirely controlled by surface and entrainment fluxes, a decrease in LE leads to a decline in cloud formation as shown by *de Arellano et al.* [2012] in a different context where CO_2 was increasing. A low evaporative fraction (i.e., the ratio between evapotranspiration to available energy) enhances ABL growth and entrainment of dry air thus leading to a decrease in RH and an increase in z_{LCL}. Even though the initial increase in z_{ABL} due to the increased

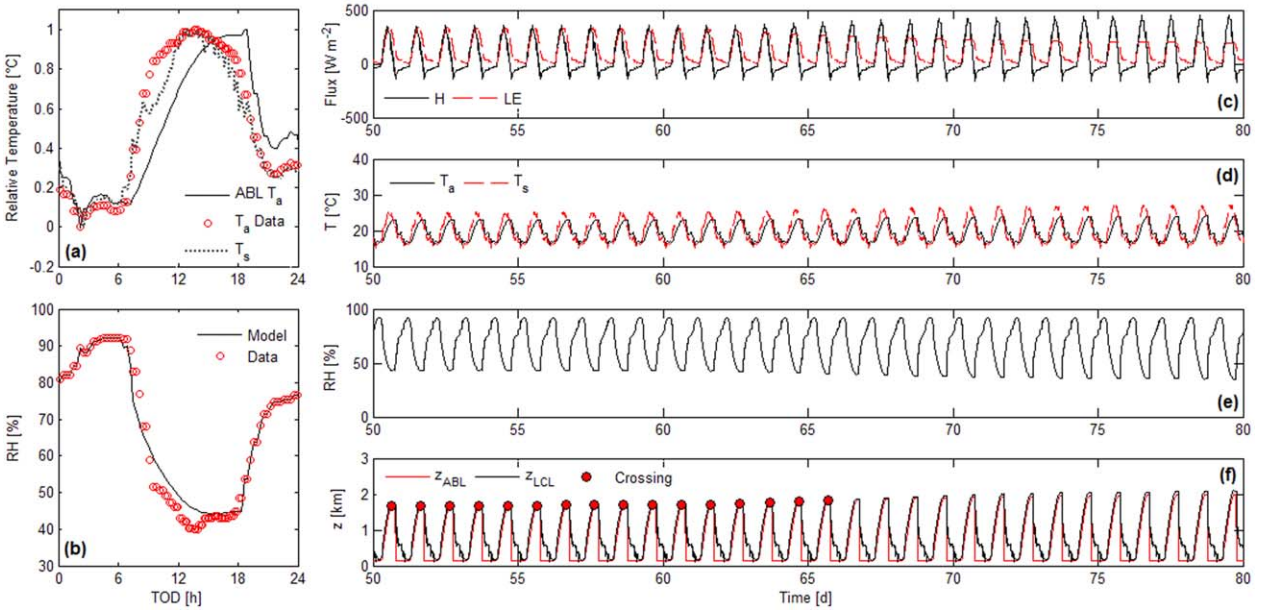

Figure 6. Simulation S2: Comparison between measured air temperature T_a, modeled air temperature in the ABL mixed layer (ML) and modeled (a) canopy temperature T_s and (b) relative humidity RH on 2 September (DOY 245) 2007. Figure 6a illustrates relative temperatures, defined as $(T-T_{min})/(T_{max}-T_{min})$. Example of fully coupled model results (Simulations S2) with water table depth set at 2.5 mbs and a humidity lapse rate set to −2.5E-6 kg/kg/m: (c) Sensible heat flux H_s and Latent heat flux LE; (d) Air Temperature T_a and canopy temperature T_s; (e) Relative humidity RH; (f) ABL and LCL heights and their crossing.

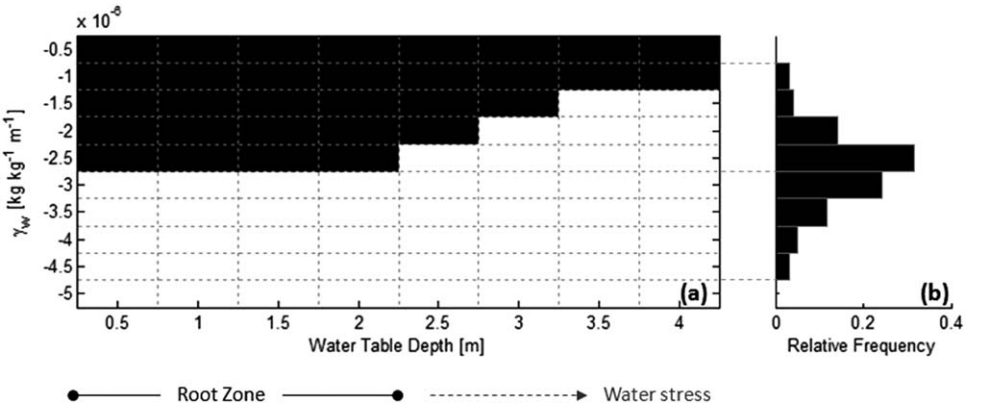

Figure 7. Simulations S2: effect of WT fluctuations on predisposition of convective rainfall by accounting for the atmospheric feedback originating from FA. The black region in Figure 7a represents ABL-LCL crossing conditions while the white region represents no-rainfall conditions. Note that the relative frequency of γ_w measured at the nearby MHX airport (daily values from June to September 2007, i.e., during the season of summertime convective rainfalls) is centered in the transition zone as shown in the histogram of measured γ_w reported in Figure 7b.

WT depth promotes predisposition to convective rainfall (positive feedback), the subsequent decrease in *RH* increases z_{LCL} and reduces the ABL-LCL crossing probability (negative feedback). To investigate the simultaneous role of WT fluctuations and FA conditions on the predisposition of convective rainfall, a sensitivity analysis is performed by varying γ_w, representing the amount of moisture available in the free atmosphere, and WT depth (Figure 7). The results demonstrate that vegetation plays a role in controlling the predisposition of rainfall only within a restricted range of γ_w. When *w* mostly originates from the FA ($\gamma_w > -1.0 \times 10^{-6}$ kg kg^{-1}m^{-1} for the present case study) vegetation exerts little control on the $z_{LCL}(t)$ height and on the ABL-LCL crossing. When the amount of moisture provided by the free atmosphere is small ($\gamma_w > -2.5 \times 10^{-6}$, for the present case study), no ABL-LCL crossing can occur no matter how shallow the water table is. Again, in this situation, vegetation does not exert any control on convective rainfall predisposition as the LCL remains consistently higher than the ABL. However, an intermediate regime exists ($-2.5 \times 10^{-6} < \gamma_w < -1.5 \times 10^{-6}$ kg kg^{-1}m^{-1} for the present case study) where vegetation can indeed promote rainfall occurrence. In this intermediate regime, transpiration can provide just enough extra atmospheric moisture to bring the system into a state where ABL-LCL crossings can occur (primarily by lowering the LCL) if the water table depth allows it. To explore the plausibility of these arguments, the FA moisture lapse rate, γ_w, was determined from linear regression of sounding profiles near the study site here (Morehead/Newport Airport, MHX data) and the outcome is presented in Figure 7b. These values were estimated from all available soundings between June and September 2007 by regressing height upon water vapor mixing ratio between elevations 0.5 and 5 km. Interestingly, the independently determined γ_w values from the sounding data here primarily fluctuated within the intermediate regime where vegetation can contribute significantly to rainfall predisposition. The results of Simulation S2 are consistent with both observations and other modeling studies. For example, *Freedman et al*. [2001] observed from data collected in the Northeastern U.S. a decrease in ABL and LCL heights with the commencement of the growing season, due to an increase in the transpiration fluxes that reduce the Bowen ratio. The study by *Freedman et al*. [2001] demonstrates that vegetation enhances cloud formation, consistent with the fully coupled vegetation-ABL system. To evaluate the role of soil water, *Kollet and Maxwell* [2008] used an integrated watershed model, arriving at the same conclusion of a positive correlation between groundwater depth and sensible heat fluxes. Similarly, *Sanchez-Mejia and Papuga* [2014] showed that the ABL height is larger over a dry soil and can decrease by up to a 1 km under wet conditions. These aforementioned studies are consistent with the results in Figure 7a. These studies were broadly focused on the role of land-surface fluxes in controlling ABL height and less on the role of FA in modifying the LCL. By tracking the crossing properties of LCL and ABL height, the simultaneous roles of land-surface fluxes and FA on predisposition of convective rainfall are unfolded.

5. Conclusions

The combined data and model results here reveal a peculiar role of WT variation on predisposition of convective rainfall. When atmospheric feedback between the soil-plant-ABL system and the ABL temperature

and humidity is censored, lowering the WT increases predisposition to convective rainfall as expected. The main pathway leading to this increase in predisposition to rainfall is that a lowered WT reduces root-water uptake, increases sensible heat flux, and subsequently leads to an expansion of the convective ABL. Because the ABL air temperature and humidity are externally imposed and not affected by land-surface or entrainment fluxes, this imposition is equivalent to forcing the LCL dynamics and decoupling them from land-surface fluxes (and WT variations). The outcome from this picture follows logical expectation: increases in ABL height in isolation translate to more frequent crossing with the LCL, thereby enhancing the predisposition to rainfall. When atmospheric feedback between the soil-plant-ABL system and the ABL temperature and humidity is allowed, the emerging outcome is more complex. The predisposition to rainfall now depends on the FA humidity state, which is governed by synoptic scale processes much larger than the ABL height. If the entrainment flux of water vapor is much larger than *LE*, then lowering WT increases the predisposition to rainfall as before (primarily because the LCL is set by moisture supplied from the free atmosphere). However, if the entrainment flux of water vapor is commensurate to or smaller than *LE*, then lowering WT reduces the predisposition to rainfall, which is opposite to the previous case. Here, the expansion in ABL height due to increases in H_s cannot "keep-up" with the rapid increases in LCL resulting from the dryer air column within the ABL due to reduced *LE*. Stated differently, if the source of water vapor within the ABL is originating from the "soil reservoir," then lowering the WT will suppress rainfall. On the other hand, if the source of water vapor in the ABL is supplied by the free atmosphere, then lowering the WT will have the opposite effect and the predisposition to rainfall is increased. While previous studies [e.g., *Maxwell et al*., 2007] noted correlations between modeled WT fluctuations on modeled surface temperature and latent heat flux and showed the signature of these correlations on boundary layer dynamics and formation of convective cells (bottom-up effects), the study here made explicit the role of the free-air state (and hence much larger weather patterns) on the predisposition of convective rainfall (top-down effects). Jointly, all these studies show that WT fluctuations, which have long memory compared to atmospheric drivers of land-surface fluxes, set the necessary conditions that enhance or ameliorate fluctuations in FA conditions favoring the onset of convective rainfall. It is to be noted that the model framework here can be extended to other ecosystems with shallow WT provided any horizontal advection in ABL water vapor or soil water is accounted for. As to the applicability of the conclusions to ecosystems with deep WT, transpiration is mainly sustained by precipitation and hence the feedbacks analyzed here are expected to be amplified.

Acknowledgments

S. Bonetti was supported by the Nicholas School of the Environment and the Pratt School of Engineering (Duke University, Durham, NC, USA). G. Manoli was supported by the University of Padova, Italy, within the Research Programme "GEO-RISKS: Geological, morphological and hydrological processes: monitoring, modelling and impact in the north-eastern Italy," WP4 and by the National Science Foundation (NSF-EAR-1344703). Domec acknowledges support from the DOE BER Terrestrial Ecosystem Sciences program (11-DE-SC-0006700 - ER65189) and the COFECUB program. Katul acknowledges support from the National Science Foundation (NSF-EAR-1344703, NSF-AGS-1102227, and NSF-CBET-103347), the United States Department of Agriculture (2011–67003-30222), the U.S. Department of Energy (DOE) through the office of Biological and Environmental Research (BER) Terrestrial Ecosystem Science (TES) Program (DE-SC0006967), and the Binational Agricultural Research and Development (BARD) Fund (IS-4374-11C). The data used in this study are available in the FLUXNET database (site: US-NC2) and can be downloaded at: http://fluxnet.ornl.gov/site/981.

References

Allen, R. G., L. S. Pereira, D. Raes, and M. Smith (1998), Crop evapotranspiration: Guidelines for computing crop requirements. Irrigation and Drainage Paper No. 56; FAO; Rome, Italy.

Aubinet, M., T. Vesala, and D. Papale (2012), *Eddy Covariance—A Practical Guide to Measurements and Data Analysis*, Springer, Netherlands.

Betts, A. K., R. L. Desjardins, and J. I. MacPherson (1992), Budget analysis of the boundary layer grid flights during FIFE 1987, *J. Geophys. Res.*, *97*, 18,533–18,534.

Brutsaert, W. (1975), On a derivable formula for long-wave radiation from clear skies, *Water Resour. Res.*, *11*, 742–744.

Camporese, M., C. Paniconi, M. Putti, and S. Orlandini (2010), Surface-subsurface flow modeling with path-based runoff routing, boundary condition-based coupling, and assimilation of multisource observation data, *Water Resour. Res.*, *46*, W02512, doi:10.1029/2008WR007536.

Chagnon, F., and R. L. Bras (2005), Contemporary climate change in the Amazon, *Geophys. Res. Lett.*, *32*, L13703, doi:10.1029/2005GL022722.

Clark, C. A., and R. W. Arritt (1995), Numerical simulations of the effect of soil moisture and vegetation cover on the development of deep convection, *J. Appl. Meteorol.*, *34*, 2029–2045.

daRocha, H. R., C. A. Nobre, J. P. Bonatti, I. R. Wright, and P. J. Sellers (1996), A vegetation atmosphere interaction study for amazonia deforestation using field data and a single column model, *Q. J. R. Meteorol. Soc.*, *122*, 567–594.

de Arellano, J. V. G., C. C. van Heerwaarden, and J. Lelieveld (2012), Modelled suppression of boundary-layer clouds by plants in a CO_2-rich atmosphere, *Nat. Geosci.*, *5*, 701–704.

Domec, J. C., J. Ogée, A. Noormets, J. Jouangy, M. J. Gavazzi, E. Treasure, G. Sun, S. G. McNulty, and J. S. King (2012), Interactive effects of nocturnal transpiration and climate change on the root hydraulic redistribution and carbon and water budgets of southern United States pine plantations, *Tree Physiol.*, *32*, 707–723.

Findell, K. L., and E. A. B. Eltahir (2003), Atmospheric controls on soil moisture-boundary layer interactions. Part II: Feedbacks within the continental United States, *J. Hydrometeorol.*, *4*, 570–583.

Foken, T. (2008), The energy balance closure problem: An overview, *Ecol. Appl.*, *18*, 1351–1367.

Freedman, J. M., D. R. Fitzjarrald, K. E. Moore, and R. K. Sakai (2001), Boundary layer clouds and vegetation-atmosphere feedbacks, *J. Clim.*, *14*, 180–197.

Garai, A., J. Kleissl, and S. G. L. Smith (2010), Estimation of biomass heat storage using thermal infrared imagery: Application to a walnut orchard, *Boundary Layer Meteorol.*, *137*, 333–342.

Garratt, J. R., and R. A. Brost (1981), Radiative cooling effects within and above the nocturnal boundary layer, *J. Atmos. Sci.*, *38*, 2730–2746.

Gentine, P., A. A. M. Holtslag, F. D'Andrea, and M. Ek (2013a), Surface and atmospheric controls on the onset of moist convection over land, *J. Hydrometeorol.*, *14*, 1443–1462.

Gentine, P., C. R. Ferguson, and A. A. M. Holtslag (2013b), Diagnosing evaporative fraction over land from boundary-layer clouds, *J. Geophys. Res. Atmos.*, *118*, 8185–8196, doi:10.1002/jgrd.50416.

Juang, J. Y., A. Porporato, P. C. Stoy, M. S. Siqueira, A. C. Oishi, M. Detto, H. S. Kim, and G. G. Katul (2007), Hydrologic and atmospheric controls on initiation of convective precipitation events, *Water Resour. Res.*, *43*, W03421, doi:10.1029/2006WR004954.
Katul, G. G., S. Manzoni, S. Palmroth, and R. Oren (2010), A stomatal optimization theory to describe the effects of atmospheric CO_2 on leaf photosynthesis and transpiration, *Ann. Bot.*, *105*, 431–442.
Katul, G. G., R. Oren, S. Manzoni, C. Higgins, and M. B. Parlange (2012), Evapotranspiration: A process driving mass transport and energy exchange in the soil-plant-atmosphere-climate system, *Rev. Geophys.*, *50*, RG3002, doi:10.1029/2011RG000366.
Kim, C. P., and D. Entekhabi (1998), Feedbacks in the land-surface and mixed-layer energy budgets, *Boundary Layer Meteorol.*, *88*, 1–21.
Kollet, S., and R. M. Maxwell (2008), Capturing the influence of groundwater dynamics on land surface processes using an integrated, distributed watershed model, *Water Resour. Res.*, *44*, W02402, doi:10.1029/2007WR006004.
Konings, A. G., G. G. Katul, and A. Porporato (2010), The rainfall-no rainfall transition in a coupled land convective atmosphere system, *Geophys. Res. Lett.*, *37*, L14401, doi:10.1029/2010GL043967.
Koster, R. D., et al. (2004), Regions of strong coupling between soil moisture and precipitation, *Science*, *305*, 1138–1140.
Manoli, G., S. Bonetti, J. C. Domec, M. Putti, G. G. Katul, and M. Marani (2014), Tree root systems competing for soil moisture in a 3d soil-plant model, *Adv. Water Resour.*, *66*, 32–42.
Manzoni, S., G. Vico, G. G. Katul, P. Fay, W. Polley, S. Palmroth, and A. Porporato (2011), Optimizing stomatal conductance for maximum carbon gain under water stress: A meta-analysis across plant functional types and climates, *Funct. Ecol.*, *25*, 456–467.
Maxwell, R. M., F. K. Chow, and S. J. Kollet (2007), The groundwater-land-surface-atmosphere connection: Soil moisture effects on the atmospheric boundary layer in fully-coupled simulations, *Adv. Water Resour.*, *30*, 2447–2466.
Meyers, T. P., and S. E. Hollinger (2004), An assessment of storage terms in the surface energy balance of maize and soybean, *Agric. For. Meteorol.*, *125*, 105–115.
Noormets, A., M. Gavazzi, S. G. McNulty, G. Sun, J.-C. Domec, J. S. King, and J. Chen (2010), Response of carbon fluxes to drought in a coastal plain loblolly pine forest, *Global Change Biol.*, *16*, 272–287.
Novick, K. A., R. Oren, P. C. Stoy, M. Siqueira, J.-C. Domec, and G. G. Katul (2009), Nocturnal evapotranspiration in eddy-covariance records from three co-located ecosystems in the Southeastern U.S.: Implications for annual fluxes, *Agric. For. Meteorol.*, *149*, 1491–1504.
Paniconi, C., and M. Putti (1994), A comparison of Picard and Newton iteration in the numerical-solution of multidimensional variably saturated flow problems, *Water Resour. Res.*, *30*, 3357–3374, doi:10.1029/94WR02046.
Pino, D., J. V. G. de Arellano, and S. W. Kim (2006), Representing sheared convective boundary layer by zeroth- and first-order-jump mixed-layer models: Large-eddy simulation verification, *J. Appl. Meteorol. Climatol*, *45*, 1224–1243.
Porporato, A. (2009), Atmospheric boundary-layer dynamics with constant Bowen ratio, *Boundary Layer Meteorol.*, *137*, 227–240.
Sanchez-Mejia, Z. M., and S. A. Papuga (2014), Observations of a two-layer soil moisture influence on surface energy dynamics and planetary boundary layer characteristics in a semiarid shrubland, *Water Resour. Res.*, *50*, 306–317, doi:10.1002/2013WR014135.
Santanello, J. A., M. A. Friedl, and M. B. Ek (2007), Convective planetary boundary layer interactions with the land surface at diurnal time scales: Diagnostics and feedbacks, *J. Hydrometeorol.*, *8*, 1082–1097.
Siqueira, M., and G. G. Katul (2010), A sensitivity analysis of the nocturnal boundary-layer properties to atmospheric emissivity formulations, *Boundary Layer Meteorol.*, *134*, 223–242.
Siqueira, M., G. G. Katul, and A. Porporato (2008), Onset of water stress, hysteresis in plant conductance, and hydraulic lift: Scaling soil water dynamics from millimeters to meters, *Water Resour. Res.*, *44*, W01432, doi:10.1029/2007WR006094.
Siqueira, M., G. G. Katul, and A. Porporato (2009), Soil moisture feedbacks on convection triggers: The role of soil-plant hydrodynamics, *J. Hydrometeorol.*, *10*, 96–112.
Sobrino, J. A., J. C. Jiménez-Muñoz, and W. Verhoef (2005), Canopy directional emissivity: Comparison between models, *Remote Sens. Environ.*, *99*, 304–314.
Stoy, P., G. G. Katul, M. B. S. Siqueira, J. Y. Juang, K. A. Novick, H. R. McCarthy, A. C. Oishi, J. M. Uebelherr, H.-S. Kim, and R. Oren (2006), Separating the effects of climate and vegetation on evapotranspiration along a successional chronosequence in the southeastern U.S., *Global Change Biol.*, *12*, 1–21.
Stull, R. B. (1988), *An Introduction to Boundary Layer Meteorology*, Springer, N. Y.
Sun, G., A. Noormets, M. J. Gavazzi, S. G. McNulty, J. Chen, J. C. Domec, J. S. King, D. M. Amatya, and R. W. Skaggs (2010), Energy and water balance of two contrasting loblolly pine plantations on the lower coastal plain of North Carolina, USA, *For. Ecol. Manage.*, *259*, 1299–1310.
Tennekes, H. (1973), A model for the dynamics of the inversion above a convective boundary layer, *J. Atmos. Sci.*, *30*, 558–567.
van Genuchten, M. T., and D. R. Nielsen (1985), On describing and predicting the hydraulic properties of unsaturated soils, *Ann. Geophys.*, *3*, 615–628.
Volpe, V., M. Marani, J. D. Albertson, and G. Katul (2013), Root hydraulic constraints on water and carbon uptake in the soil-plant system under current and future climate, *Adv. Water Resour.*, *60*, 110–120.
Wallace, J. H., and P. V. Hobbs (Eds.) (2006), *Atmospheric Science: An Introductory Survey*, Academic, San Diego, Calif.